

Supporting information for “**Loquacious-PD regulates the terminus-dependent molecular recognition of Dicer-2 toward double-stranded RNA**”

McKenzie Jonely¹, Raushan K. Singh², Helen M. Donelick² Brenda L. Bass², Rodrigo Noriega^{1*}

¹ University of Utah, Department of Chemistry, Salt Lake City, UT 84112

² University of Utah, Department of Biochemistry, Salt Lake City, UT 84112

* Email: noriega@chem.utah.edu

Contents

Materials and samples	Page S2
Verification of interaction of dmDcr-2 ^{WT} and Loqs-PD with Cy3-labelled dsRNA	Page S4
Time-resolved fluorescence setup.....	Page S5
Rationale for observed probe photophysics.....	Page S6
Rotationally-averaged fluorescence and fluorescence anisotropy calculation	Page S7
Average fluorescence lifetime.....	Page S8
Fitting the fluorescence anisotropy traces.....	Page S9
Potential contributions of siRNA products to observed dynamics.....	Page S10
Time resolved fluorescence and anisotropy of dsRNA•dmDcr 2 ^{WT} •Loqs-PD complexes	Page S12
Spectroscopic validation of a distinct molecular environment due to the formation of dsRNA•dmDcr 2 ^{WT} •Loqs-PD complexes	Page S13
Supplemental References.....	Page S15

Materials and samples. All proteins used in this work have been previously described:¹⁻⁵

- dmDcr-2^{WT} is the full-length, wild type of *Drosophila melanogaster* Dicer-2 (**Fig. S1**).
- dmDcr-2^{RIII} differs from dmDcr-2^{WT} in two point mutations: D1217A (RIIIa domain) and D1476A (RIIIb domain).
- this work employs the full-length Loqs-PD protein.

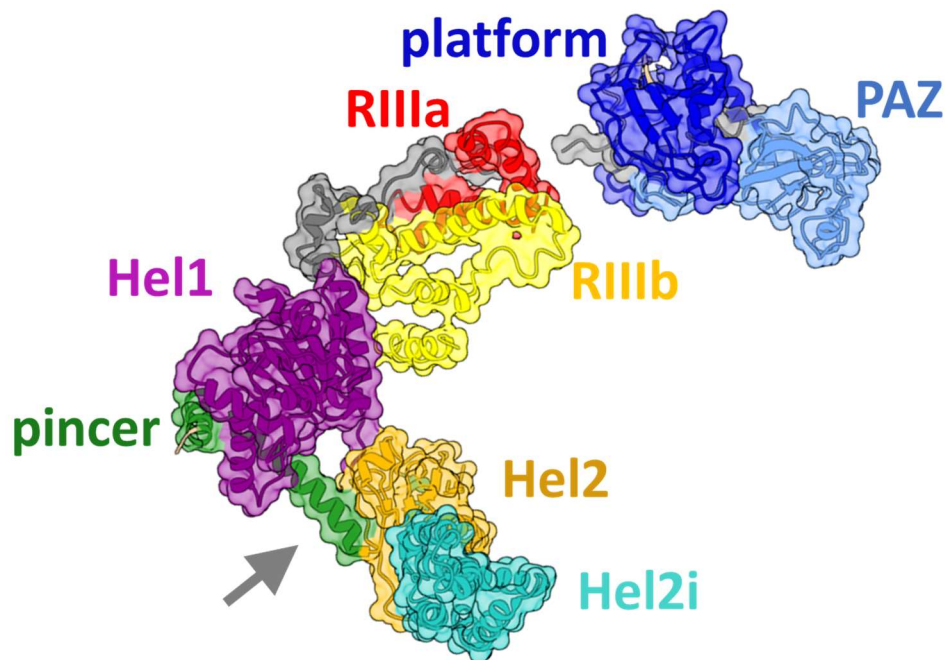


Figure S1. Structure of apo dmDcr-2 (PDB: 6BUA) with its tandem RNase III domains (RIIIa, RIIIb), helicase subdomains (Hel1, Hel2, and Hel2i), and its pincer, platform, and PAZ (Piwi-Argonaute-Zwille) domains labelled. The open helicase pocket is shown (arrow).

Protein variants, expression, and purification. All proteins in this work were expressed and purified using a modified pFastBacTM protocol previously described in detail.⁶

Nucleic acid synthesis and preparation. As previously described,⁵ antisense RNA strands were synthesized and purified at the DNA/Peptide Facility, part of the Health Science Center Cores at the University of Utah. Sense strands were purchased from Integrated DNA Technologies.

Unidirectional binding of dsRNA by dmDcr-2 was favored with a dual approach, which has been

previously detailed in the literature. In all substrates employed, binding at one terminus of the dsRNA construct was blocked with two deoxynucleotides at the 3' end of the sense strand,^{1,2,7-9} and with a biotin modification at the 5' end of the antisense strand.^{1,2,10} As a result, any changes observed in the local environment of the Cy3 probe are due to binding of the fluorescently labeled terminus. Sense and antisense strand sequences are below.

52-nt Sense strand (deoxynucleotides underlined)

5'-Cy3-GGAGGUAGUAGGUUGUAUAGUAGUAAGACCAGACCCUAGACCAAUUCAUGCC-3'

52-nt blunt Antisense strand

Biotin-5'-GGCAUGAAUUGGUCUAGGGUCUGGUCUUACUACUAUACAACCUACUACCUCC-3'

54-nt 3'overhang Antisense strand

Biotin-5'-GGCAUGAAUUGGUCUAGGGUCUGGUCUUACUACUAUACAACCUACUACCUCCAA-3'

To prepare dsRNAs from the single RNA strands above, equimolar amounts of 52-nt sense strands and either 52-nt or 54-nt antisense strands (for blunt or 3'overhang, respectively) were mixed in annealing buffer (50 mM Tris pH 8.0, 20mM KCl). Mixtures were heated at 95°C for 2 min and allowed to cool to room temperature for 4 h before purification after 8% native PAGE.

Nucleotide. ATP- γ S, a non-hydrolysable version of ATP, was purchased from Sigma-Aldrich and used as received.

Replicate samples. For each condition tested, multiple trials were measured with independently prepared replicates in separate data acquisition sessions.

Transients previously reported in the literature. Time-resolved fluorescence and anisotropy traces for two of the samples discussed in the Main Text (1 out of 3 repeats of the unbound dsRNA constructs) were previously reported in a manuscript focusing on the transient kinetics of dmDcr-2^{RIII}.⁵ Here, we only include their photophysical parameters ($\langle\tau\rangle$, $r(\infty)/r(0)$, and τ_{rot}) in order to maximize the sample size for the purposes of comparing modes of binding. For the

comparison to the non-cleaving mutant dmDcr-2^{RIII} (**Fig. S3** on this ESI document) we also include the $\langle\tau\rangle$, $r(\infty)/r(0)$, and τ_{rot} values only – the fluorescence decay and transient anisotropy of the 3'overhang•dmDcr-2^{RIII} and 3'overhang•dmDcr-2^{WT}•ATP- γ S can be found in Ref. [5] None of the time resolved traces shown in any of the figures in this manuscript have been previously published.

Verification of interaction of dmDcr-2^{WT} and Loqs-PD with Cy3-labelled dsRNA. To

provide independent evidence of binding of Cy3-labelled substrates by dmDcr-2^{WT} and Loqs-PD, we have conducted electrophoretic mobility shift assays (**Fig. S2**), which validate the formation of dsRNA•dmDcr-2^{WT}•Loqs-PD complexes with both blunt and 3'overhang dsRNA. Electrophoretic mobility shift assays were performed using dmDcr-2 (1 μ M-2 μ M, wild type for blunt dsRNA, RNase III mutant for 3' ovr dsRNA) and wild type Loqs-PD (1 μ M-2 μ M). Reactions were performed with a 5' Cy3 end-labeled 52mer dsRNA for both blunt (BLT) and 3' overhang (0.5 μ M-2 μ M). If both dmDcr-2^{WT} and Loqs-PD were included in the reaction, the proteins were pre-equilibrated for 10 min before the addition of dsRNA and ATP. dsRNA was prepared as previously described (details above in this ESI).⁵ dsRNA was incubated with the protein(s) (4°C, 30 min, in the dark) in the presence of ATP with equal molar Mg²⁺ (5 mM) in 10 μ L binding assay buffer (25 mM TRIS pH 8.0, 100 mM KCl, 10 mM MgCl₂•6H₂O, 10% (vol/vol) glycerol, 1 mM TCEP), to achieve equilibrium. Reactions were stopped by loading the reaction onto a 4% (29:1acrylamide/bisacrylamide) native gel running at 150 V, 4°C in 0.5x Tris/borate/EDTA. Gels were electrophoresed in the dark to resolve bound dsRNA from free dsRNA for 3.5 hours. Gels were imaged using the green channel (532 nm) on a Typhoon TRIO Variable Mode Imager (Amersham Bioscience) in the linear dynamic range of the instrument using ImageQuant TL version 7 software.

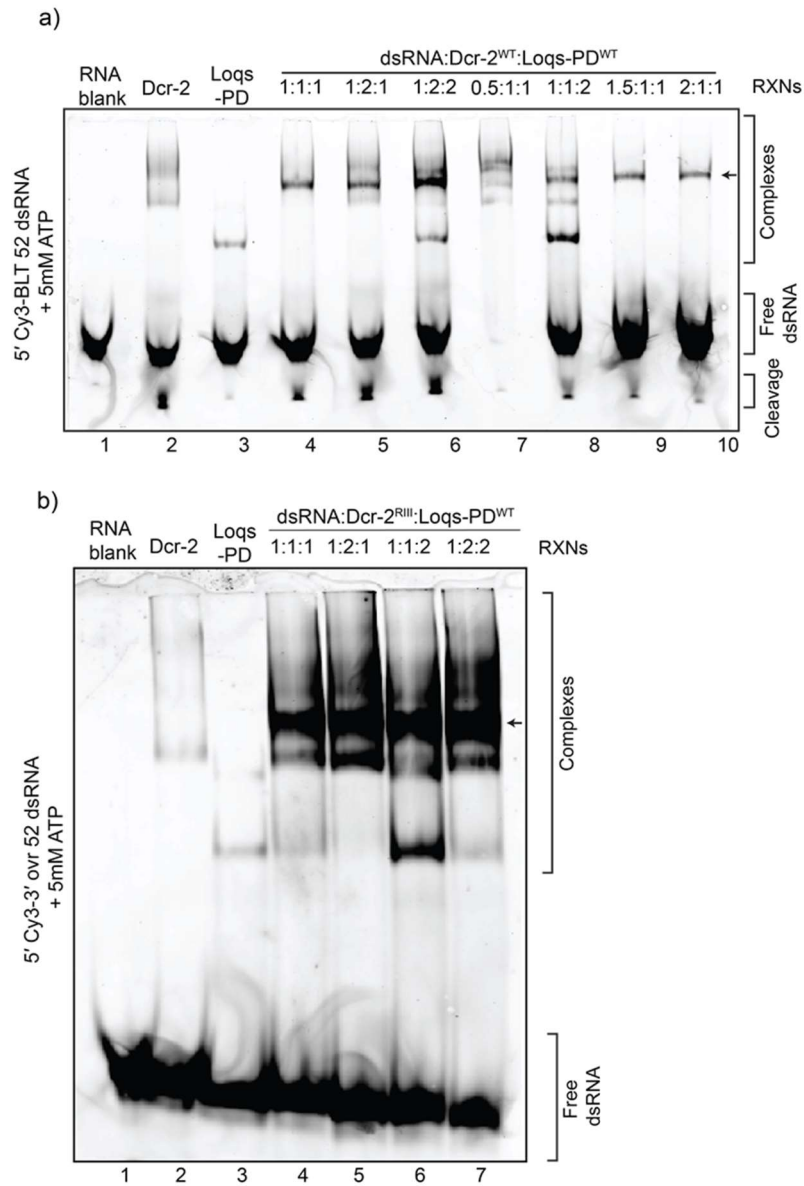


Figure S2. Electrophoretic mobility shift assay of **(a)** dmDcr-2^{WT} with 5' Cy3 blunt (BLT) 52mer dsRNA, n=7 and **(b)** dmDcr-2^{RIII} with 5' Cy3 3' ovr 52mer dsRNA, n=1. Wild type Loqs-PD was used in both **(a)** and **(b)**, and all reactions included 5 mM ATP with equal molar Mg²⁺. Reaction ratios are the micromolar ratios of dsRNA:dmDcr-2:Loqs-PD. Arrows point to unique bands corresponding to the complex of dsRNA•dmDcr-2•Loqs-PD.

Time-resolved fluorescence data collection. The polarization-resolved epifluorescence setup employed in this work has been previously described.⁵ Data were collected in three separate sessions. For the initial session, the instrument resolution was set to 4 ps and each trace was

integrated over 900 s; subsequent data sets were collected with a resolution of 16 ps and 110 s integration time. These instrumental parameters were modified to maintain a large signal to noise ratio in the time-resolved data while reducing the possibility of photodamage in long-duration acquisitions, and their modification did not affect the measurement results. In each experimental run, we measured freely-diffusing Cy3 chromophores in solution as a control sample. Small-volume aliquots for fluorescence experiments were prepared immediately before use and contain 0.2 μM of Cy3 end-labeled dsRNA and, if used: 2 μM of dmDcr-2 protein, 2 μM of Loqs-PD, and 8 mM of ATP- γS . Samples were allowed to equilibrate for 5 min. prior to time-resolved fluorescence measurements.

Rationale for observed probe photophysics. Fluorescent probes as reporters of local conditions have been used extensively in biophysical studies, with a wide array of chromophores that serve as polarity, pH, viscosity, and ion concentration sensors.¹¹⁻¹⁹ Typical spectroscopic observables include brightness, absorption/emission lineshapes, fluorescence lifetime, and steady-state or time-resolved fluorescence anisotropy. In this study, we employ a combination of time-resolved photophysical observables of an indocarbocyanine dye (Cy3) to determine its intramolecular and intermolecular measures of rigidity. Photoexcited indocarbocyanine dyes are known to undergo a cis-trans isomerization of their polymethine chain, which results in an efficient nonradiative decay pathway. When the local environment of indocarbocyanine dyes becomes more rigid, their excited state isomerization is hindered, which is reflected in an extension of their fluorescence lifetime and an increase in their brightness.²⁰⁻²⁴ This effect has been observed in homogeneous bulk solutions in a viscosity- and temperature-dependent manner, and it is the basis of protein-induced fluorescence enhancement effects.²⁵ It is also important to consider the initial state of the

fluorophore conjugate (e.g., Cy3-labeled nucleic acids), since the disruption of its initial state can also lead to protein-induced fluorescence quenching.²⁶

Beyond these excited state decay dynamics that primarily reflect an intramolecular process, collective processes can reveal important local environment properties – e.g., time-resolved fluorescence anisotropy.^{27,28} A linearly polarized pump laser preferentially excites molecules whose transition dipole moments are aligned with its polarization, creating an anisotropic distribution of excited state dipoles even in an otherwise isotropic sample. If dye molecules are able to reorient in space (e.g., rotations perpendicular to the transition dipole moment) this initially-anisotropic distribution of excited state dipoles de-polarizes over a characteristic rotational diffusion time that depends on the hydrodynamic radius of the rotating emitter. When rotation is unimpeded, the long-time average polarization is negligible. However, if the reorientation of the emitters is hindered, a nonzero anisotropy can remain present at long times. This restricted motion is typically observed for dye-labeled nucleic acid-protein complexes, where the rotational diffusion of a chromophore also involves its immediate solvation shell, the macromolecule to which it is covalently attached, and nearby protein segments.²⁷

Rotationally-averaged fluorescence and fluorescence anisotropy calculation. Raw data consists of the number of photons detected at each delay time (12.5 ns time window given by our laser repetition rate), tagged by detection channel (vertical or horizontal polarization). All data processing and analysis was performed in MATLAB. Differences in the optical path length from the sample to each photodiode and in the length of cables connecting each detector to routing and photon counting electronics require a small (~0.38 ns), constant shift in the relative time axis for both channels. A nonzero baseline due to dark counts and background photons was subtracted

prior to further processing. After these pre-processing steps, data for vertical and horizontal polarization channels, $I_{VV}(t)$ and $I_{VH}(t)$ respectively, was used to calculate the rotationally-averaged fluorescence, $I_{tot}(t)$, and the fluorescence anisotropy, $r(t)$:

$$I_{tot}(t) = gI_{VV}(t) + 2I_{VH}(t) \quad \text{Eq. S1}$$

$$r(t) = \frac{(gI_{VV}(t) - I_{VH}(t))}{(gI_{VV}(t) + 2I_{VH}(t))} \quad \text{Eq. S2}$$

Differences in the collection efficiency for the two detection channels (e.g., fiber and detector coupling efficiencies) were equalized with a scaling factor g , whose value is set to ensure each sample's initial anisotropy equals $r(0) = 0.4$, as expected for a 3-dimensional isotropic distribution of transition dipole moments prior to excitation.¹¹ The V/H channel equalization factor g is an instrument variable that can be affected by slight changes in alignment. However, within each experimental session, the values for g do not change drastically (standard deviation is at most 12% of the average value).

Average fluorescence lifetime. Free Cy3 in phosphate buffer solution has a short fluorescence lifetime – comparable to the finite duration of the instrument response function for our setup. For these samples, the rotationally-averaged fluorescence traces of Cy3 samples were described by a single exponential decay in a nonlinear least-squares fitting algorithm, yielding an emission lifetime of $\tau_{\text{Cy3}} = 310 \pm 1$ ps. All other samples had significantly slower fluorescence decays with substantial photon counts at times much longer than the instrumental response. Therefore, the average fluorescence lifetime for Cy3 labels in all dsRNA samples (with or without protein) were calculated numerically based on the intensity-weighted photon arrival time (**Eq. S3**). The average fluorescence lifetimes obtained in this way for samples containing 3' overhang or blunt dsRNA are shown in **Table S1**.

$$\langle \tau \rangle = \frac{\sum_i t_i I_{tot}(t_i)}{\sum_i I_{tot}(t_i)} \quad \text{Eq. S3}$$

Table S1. Fluorescence lifetime (values in ns) for all individual samples, grouped by sample type. Uncertainties are standard error propagated from raw data (Poisson counting statistics).

	blunt	3'overhang
dsRNA	1.525 ± 0.001	1.364 ± 0.001
	1.471 ± 0.005	1.276 ± 0.007
	1.146 ± 0.005	1.264 ± 0.005
dsRNA•dmDcr-2 ^{WT}	1.614 ± 0.001	1.395 ± 0.001
	1.579 ± 0.005	1.305 ± 0.006
dsRNA•dmDcr-2 ^{WT} •ATP-γS	1.913 ± 0.001	1.414 ± 0.001
	2.001 ± 0.005	1.335 ± 0.006
dsRNA•dmDcr-2 ^{WT} •Loqs-PD	1.811 ± 0.001	1.605 ± 0.001
	1.816 ± 0.005	1.562 ± 0.006
dsRNA•dmDcr-2 ^{WT} •Loqs-PD•ATP-γS	1.895 ± 0.001	1.664 ± 0.001
	2.043 ± 0.005	1.993 ± 0.007

Fitting the fluorescence anisotropy traces. Being attached to a large RNA molecule (even in the absence of biomolecular complex formation) restricts the freedom of motion of the Cy3 fluorophore, so the residual anisotropy displayed by these samples is considerable, $0.22 < r(\infty) < 0.36$. The relatively small decay in the anisotropy, together with the fact that transient anisotropy is extracted from the difference between individual fluorescence traces and thus more susceptible to noise, limits our ability to accurately determine multi-exponential anisotropy decay. While in some cases a very weak and fast component (<10% of the total amplitude and sub-ns time scale) is observed, the anisotropy loss and asymptotic anisotropy values, Δr and $r(\infty)$, are not noticeably affected. Thus, a single exponential description of the entire decay (data in the 0-4.5 ns range) was chosen for all samples, and the fitted rotational diffusion time τ_{rot} can be understood as the average time scale for the population of excited chromophores to reach their “equilibrium” anisotropy value, $r(\infty)$. The transient anisotropy trace for each sample was described with a single exponential decay and a long-time baseline (Eq. S4) using a nonlinear least-squares algorithm.

$$r(t) = \Delta r e^{-t/\tau_{\text{rot}}} + r(\infty) \quad \text{Eq. S4}$$

Free Cy3 samples display a negligible residual anisotropy $r(\infty) = 0.06 \pm 0.04$ and a short rotational diffusion time $\tau_{\text{rot}} = 0.43 \pm 0.02$ ns, as expected for small, freely diffusing chromophores.¹¹ Chromophores labeling dsRNA termini (with or without protein binding) have substantially slower rotational diffusion times and larger residual anisotropy values – fit parameters for their transient fluorescence anisotropy traces are reported in **Table S2** below.

Table S2. Transient fluorescence anisotropy fits for all individual samples, grouped by sample type. Uncertainties are standard error from nonlinear fitting.

	blunt			
	Δr	τ_{rot} (ns)	$r(\infty)$	$r(\infty)/r(0)$
dsRNA	0.122 ± 0.001	1.52 ± 0.05	0.278 ± 0.001	0.695 ± 0.004
	0.146 ± 0.005	1.1 ± 0.1	0.242 ± 0.004	0.62 ± 0.01
	0.185 ± 0.008	1.6 ± 0.2	0.228 ± 0.009	0.55 ± 0.03
dsRNA•dmDcr-2 ^{WT}	0.099 ± 0.001	1.37 ± 0.04	0.300 ± 0.001	0.752 ± 0.003
	0.134 ± 0.005	1.05 ± 0.09	0.258 ± 0.003	0.66 ± 0.01
dsRNA•dmDcr-2 ^{WT} •ATP- γ S	0.064 ± 0.001	1.13 ± 0.04	0.338 ± 0.001	0.841 ± 0.002
	0.073 ± 0.003	1.1 ± 0.1	0.332 ± 0.003	0.82 ± 0.01
dsRNA•dmDcr-2 ^{WT} •Loqs-PD	0.066 ± 0.001	1.23 ± 0.04	0.333 ± 0.001	0.834 ± 0.003
	0.085 ± 0.004	1.0 ± 0.1	0.315 ± 0.003	0.79 ± 0.01
dsRNA•dmDcr-2 ^{WT} •Loqs-PD•ATP- γ S	0.063 ± 0.001	1.21 ± 0.04	0.335 ± 0.001	0.842 ± 0.002
	0.067 ± 0.003	1.0 ± 0.1	0.315 ± 0.002	0.82 ± 0.01
	3'overhang			
	Δr	τ_{rot} (ns)	$r(\infty)$	$r(\infty)/r(0)$
dsRNA	0.113 ± 0.001	1.36 ± 0.05	0.284 ± 0.001	0.715 ± 0.005
	0.17 ± 0.01	1.8 ± 0.3	0.24 ± 0.01	0.59 ± 0.03
	0.162 ± 0.008	1.9 ± 0.3	0.244 ± 0.009	0.60 ± 0.03
dsRNA•dmDcr-2 ^{WT}	0.103 ± 0.001	1.39 ± 0.05	0.290 ± 0.001	0.738 ± 0.003
	0.144 ± 0.006	1.1 ± 0.1	0.236 ± 0.004	0.62 ± 0.02
dsRNA•dmDcr-2 ^{WT} •ATP- γ S	0.094 ± 0.001	1.18 ± 0.04	0.294 ± 0.001	0.757 ± 0.004
	0.146 ± 0.007	1.6 ± 0.2	0.257 ± 0.008	0.64 ± 0.03
dsRNA•dmDcr-2 ^{WT} •Loqs-PD	0.055 ± 0.001	0.77 ± 0.04	0.344 ± 0.001	0.862 ± 0.003
	0.079 ± 0.006	0.9 ± 0.2	0.309 ± 0.003	0.80 ± 0.02
dsRNA•dmDcr-2 ^{WT} •Loqs-PD•ATP- γ S	0.051 ± 0.002	0.67 ± 0.04	0.343 ± 0.001	0.871 ± 0.004
	0.037 ± 0.007	0.5 ± 0.2	0.361 ± 0.002	0.91 ± 0.02

Potential contributions by siRNA products to observed dynamics. The wild type dmDcr-2 enzyme used in this work has active RNase III cleaving sites that can result in the production of

siRNA from the 3' overhang dsRNA substrates (although it is not an optimal substrate). Thus, the fluorescence signal measured in our long-time equilibrium experiments can include contributions from siRNA products. However, we find that these contributions are not large enough to undermine the connection between local environment at the dsRNA terminus and the dominant mode of molecular recognition. This conclusion is supported by comparison to a non-cleaving mutant, dmDcr-2^{RIII}. The trend in local environment as dmDcr-2^{RIII} binds 3' overhang dsRNA with and without ATP- γ S is very similar to that observed with the wild type enzyme, dmDcr-2^{WT} (Fig. S3). These similarities are maintained both in the presence and absence of Loqs-PD.

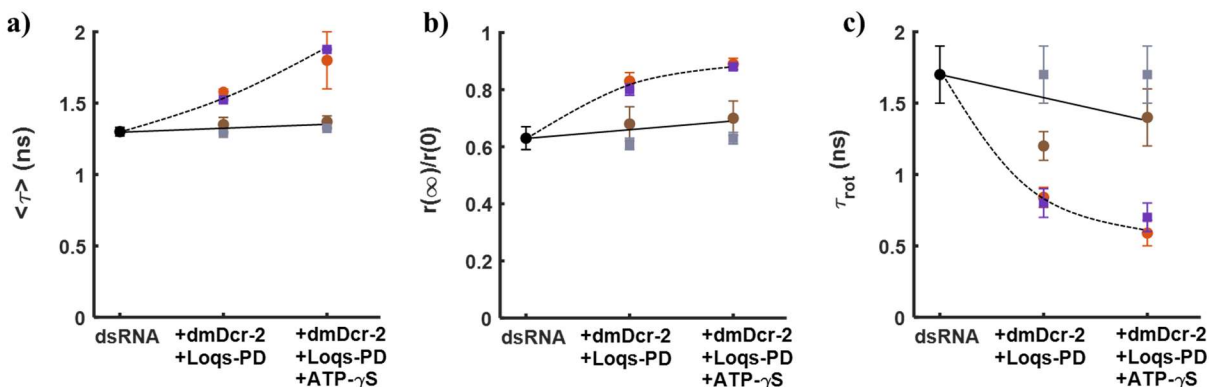


Figure S3. The average fluorescence lifetime (a), residual anisotropy (b), and rotational diffusion time (c) of a Cy3 probe show that the local binding environment at the 3' overhang dsRNA terminus when bound by dmDcr-2^{WT} (circles) and dmDcr-2^{RIII} mutant (squares) show similar progressions, both in the absence of Loqs-PD (brown and gray) and in the presence of Loqs-PD (orange and purple). The common point of comparison, 3' overhang dsRNA, is shown in black. Black solid and dotted lines are guides to more easily identify trends. For dsRNA and dmDcr-2^{WT} results, markers are averages of $N = 2 - 3$ trials and error bars are the standard error of the mean. For dmDcr-2^{RIII} results, markers are extracted values from an individual measurement and error bars are propagated uncertainty from data.

Time resolved fluorescence and anisotropy data of dsRNA•dmDcr-2^{WT}•Loqs-PD

complexes. The photophysical parameters of Cy3 probes at dsRNA termini upon their binding by dmDCR-2^{WT} in the presence of Loqs-PD, as shown in Main Text **Fig. 2**, are extracted from time-resolved data as shown below in **Fig. S4**. These traces are provided here as a visual comparison to the time-resolved data in the absence of Loqs-PD (**Fig. 1a-d** in Main Text).

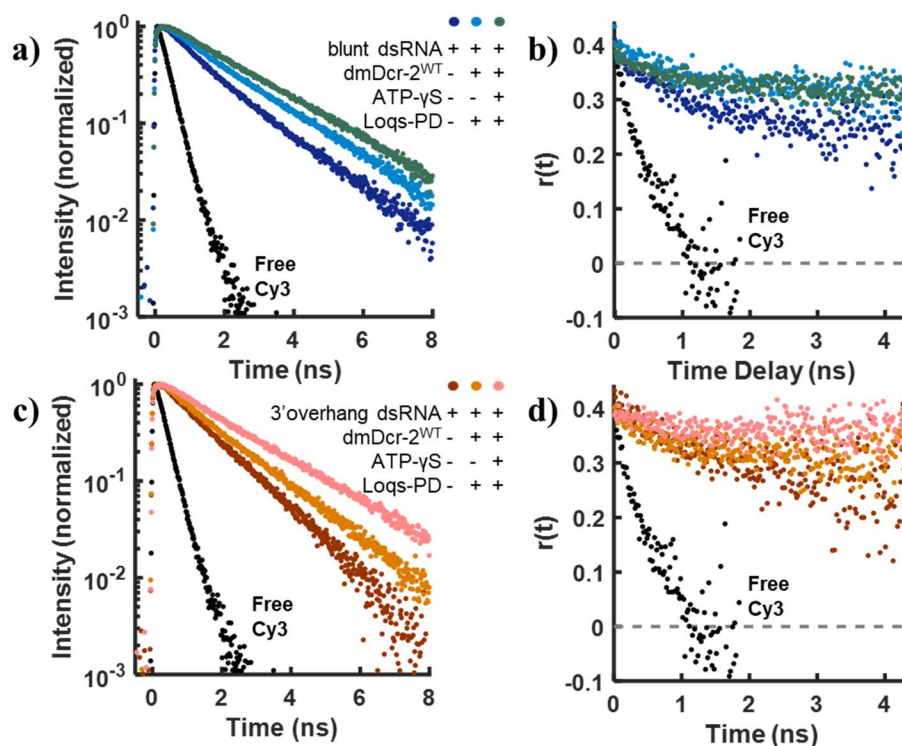


Figure S4. (a,c) Rotationally-averaged fluorescence intensity, and (b,d) time-resolved fluorescence anisotropy for Cy3 chromophores covalently attached to blunt (a,b) or 3'overhang dsRNA (c,d) as they interact with dmDcr-2^{WT} in the presence of Loqs-PD. Fluorescence and transient anisotropy of free Cy3 in solution shown as a reference (black).

Spectroscopic validation of a distinct molecular environment due to the formation of dsRNA•dmDcr-2^{WT}•Loqs-PD complexes.

The spectroscopic observation of a dsRNA•dmDcr-2•Loqs-PD complex (as opposed to binding of dsRNA by dmDcr-2^{WT} or Loqs-PD only) is further supported by comparing experiments where the fluorescence dynamics of Cy3-labelled dsRNA are monitored upon binding by Loqs-PD alone or dmDcr-2^{WT} alone to those for the full dsRNA•dmDcr-2•Loqs-PD complex (**Fig. S5**). For both types of dsRNA termini, the fluorescence lifetime and residual fluorescence anisotropy are larger when the full dsRNA•dmDcr-2^{WT}•Loqs-PD complex is formed (compared to the values for the pairwise interactions dsRNA•dmDcr-2^{WT} or dsRNA•Loqs-PD). Similarly, the rotational diffusion times are faster when the full dsRNA•dmDcr-2^{WT}•Loqs-PD complex is formed (compared to the values for the pairwise interactions dsRNA•dmDcr-2^{WT} or dsRNA•Loqs-PD). These results show that the local environment at the dsRNA terminus when both proteins are present is distinct from that observed when only one protein interacts with the dsRNA. Together with the gel shift experiments described above (**Fig. S2**), these supporting experiments validate our interpretation that the results in **Fig. 2** on the Main Text reflect the local environment at the dsRNA termini upon the formation of dsRNA•dmDcr-2^{WT}•Loqs-PD complexes.

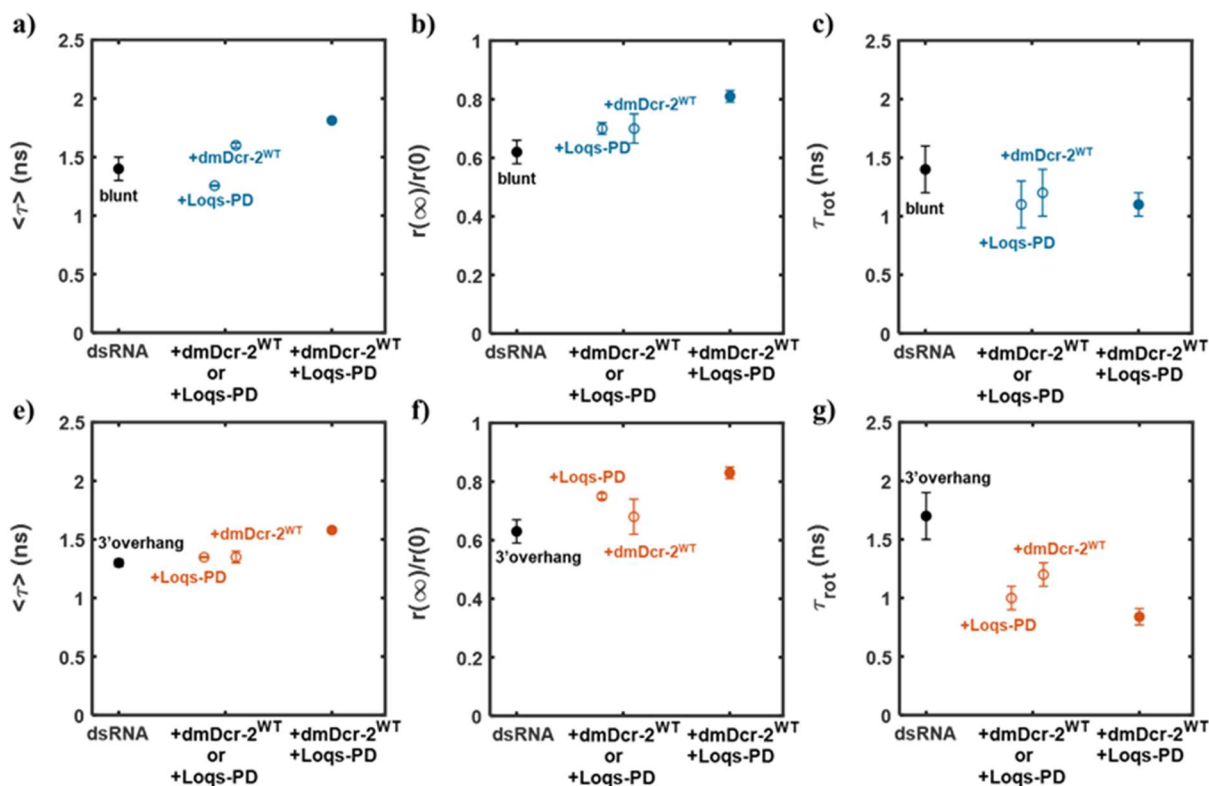


Figure S5. Photophysical parameters of fluorescently-labeled dsRNA substrates in the presence of dmDcr-2^{WT}, Loqs-PD, or both proteins. The average fluorescence lifetime (**a** for blunt, **e** for 3'overhang), ratio of asymptotic to initial fluorescence anisotropy (**b** for blunt, **f** for 3'overhang), and rotational diffusion time (**c** for blunt, **g** for 3'overhang) show that the dsRNA•dmDcr-2^{WT}•Loqs-PD complex displays a distinct local environment and is not the result of partially formed complexes. Data for dsRNA, dsRNA•dmDcr-2^{WT}, and dsRNA•dmDcr-2^{WT}•Loqs-PD are those shown in **Figs. 1-2** in the Main Text. Data for dsRNA•Loqs-PD show fitted values and error bars are their $\pm\sigma$ confidence intervals.

Supplemental References

- 1 N. K. Sinha, J. Iwasa, P. S. Shen and B. L. Bass, *Science*, 2018, **359**, 329–334.
- 2 H. M. Donelick, L. Talide, M. Bellet, J. Aruscavage, E. Lauret, E. Aguiar, J. T. Marques, C. Meignin and B. L. Bass, *RNA*, 2020, **26**, 1847–1861.
- 3 N. K. Sinha, K. D. Trettin, P. J. Aruscavage and B. L. Bass, *Mol. Cell*, 2015, **58**, 406–417.
- 4 K. D. Trettin, N. K. Sinha, D. M. Eckert, S. E. Apple and B. L. Bass, *PNAS*, 2017, **114**, E7939–E7948.
- 5 R. K. Singh, M. Jonely, E. Leslie, N. A. Rejali, R. Noriega and B. L. Bass, *eLife*, 2021, **10**, e65810.
- 6 N. K. Sinha and B. L. Bass, *Methods*, 2017, **126**, 54–65.
- 7 E. S. Cenik, R. Fukunaga, G. Lu, R. Dutcher, Y. Wang, T. M. Tanaka Hall and P. D. Zamore, *Molecular Cell*, 2011, **42**, 172–184.
- 8 S. D. Rose, D.-H. Kim, M. Amarguioui, J. D. Heidel, M. A. Collingwood, M. E. Davis, J. J. Rossi and M. A. Behlke, *Nucleic Acids Res*, 2005, **33**, 4140–4156.
- 9 R. Fukunaga, C. Colpan, B. W. Han and P. D. Zamore, *The EMBO Journal*, 2014, **33**, 371–384.
- 10 C. L. Noland, E. Ma and J. A. Doudna, *Molecular Cell*, 2011, **43**, 110–121.
- 11 J. R. Lakowicz, *Principles of Fluorescence Spectroscopy*, Springer, Third., 2006.
- 12 P. K. Mandal and A. Samanta, *J. Phys. Chem. B*, 2005, **109**, 15172–15177.
- 13 R. Das, D. Guha, S. Mitra, S. Kar, S. Lahiri and S. Mukherjee, *J. Phys. Chem. A*, 1997, **101**, 4042–4047.
- 14 Z. Zhujun and W. R. Seitz, *Analytica Chimica Acta*, 1984, **160**, 47–55.
- 15 L. A. Saari and W. R. Seitz, 3.
- 16 X. Peng, Z. Yang, J. Wang, J. Fan, Y. He, F. Song, B. Wang, S. Sun, J. Qu, J. Qi and M. Yan, *J. Am. Chem. Soc.*, 2011, **133**, 6626–6635.
- 17 M. A. Haidekker, T. P. Brady, D. Lichlyter and E. A. Theodorakis, *J. Am. Chem. Soc.*, 2006, **128**, 398–399.
- 18 H.-Y. Lin, P.-Y. Cheng, C.-F. Wan and A.-T. Wu, *Analyst*, 2012, **137**, 4415–4417.
- 19 G. Crivat, K. Kikuchi, T. Nagano, T. Priel, M. Hershfinkel, I. Sekler, N. Rosenzweig and Z. Rosenzweig, *Anal. Chem.*, 2006, **78**, 5799–5804.
- 20 E. Åkesson, V. Sundström and T. Gillbro, *Chemical Physics Letters*, 1985, **121**, 513–522.
- 21 J. Widengren and P. Schwille, *J. Phys. Chem. A*, 2000, **104**, 6416–6428.
- 22 K. Jia, Y. Wan, A. Xia, S. Li, F. Gong and G. Yang, *J. Phys. Chem. A*, 2007, **111**, 1593–1597.
- 23 E. M. S. Stennett, N. Ma, A. van der Vaart and M. Levitus, *J. Phys. Chem. B*, 2014, **118**, 152–163.
- 24 S. M. Hart, J. L. Banal, M. Bathe and G. S. Schlau-Cohen, *J. Phys. Chem. Lett.*, 2020, **11**, 5000–5007.
- 25 E. M. S. Stennett, M. A. Ciuba, S. Lin and M. Levitus, *J. Phys. Chem. Lett.*, 2015, **6**, 1819–1823.
- 26 F. Rashid, V.-S. Raducanu, M. S. Zaher, M. Tehseen, S. Habuchi and S. M. Hamdan, *Nat Commun*, 2019, **10**, 2104.
- 27 M. E. Sanborn, B. K. Connolly, K. Gurunathan and M. Levitus, *J. Phys. Chem. B*, 2007, **111**, 11064–11074.
- 28 J. Spiriti, J. K. Binder, M. Levitus and A. van der Vaart, *Biophys. J.*, 2011, **100**, 1049–1057.